Light: Science & Applications (2015) 4, e330; doi:10.1038/lsa.2015.103
© 2015 CIOMP. All rights reserved 2047-7538/15
www.nature.com/lsa

ORIGINAL ARTICLE

Plasmonic polarization generator in well-routed beaming

Lin Li[1,2], Tao Li[1,2], Xia-Mei Tang[1,2], Shu-Ming Wang[1,2], Qian-Jin Wang[1,2] and Shi-Ning Zhu[1,2]

As one of the recent advances of optics and photonics, plasmonics has enabled unprecedented optical designs. Having a vectorial configuration of surface plasmon field, metallic nanostructures offer efficient solutions in polarization control with a very limited sample thickness. Many compact polarization devices have been realized using such metallic nanostructures. However, in most of these devices, the functions were usually simple and limited to a few polarization states. Here, we demonstrated a plasmonic polarization generator that can reconfigure an input polarization to all types of polarization states simultaneously. The plasmonic polarization generator is based on the interference of the in-plane (longitudinal) field of the surface plasmons that gives rise to versatile near-field polarization states on a metal surface, which have seldom been considered in previous studies. With a well-designed nanohole array, the in-plane field of SPPs with proper polarization states and phases can be selectively scattered out to the desired light beams. A manifestation of eight focusing beams with well-routed polarizations was experimentally demonstrated. Our design offers a new route to achieve the full control of optical polarizations and possibly advance the development in photonic information processing.

Light: Science & Applications (2015) **4,** e330; doi:10.1038/lsa.2015.103; published online 25 September 2015

Keywords: near-field interference; phase modulation; plasmonics; polarization generator

INTRODUCTION

Optical polarization is an important characteristic of light that enables transmission of information for signal processing in optical information technology by utilizing classical or quantum phenomena. Compared with conventional optical elements, plasmonic devices provide a more compact and efficient means to manipulate the polarization of light (e.g., plasmonic polarizers[1–5], polarization rotators and converters[6–11], polarization detectors[12], etc.). Recently, plasmon-induced spin-orbital coupling has generated strong interest in the field of photonics[13–17], primarily due to the possibility of polarization and phase modulation. In fact, the vectorial structure of the surface plasmon field gives rise to unique properties in the conversion of optical fields between propagating light and bounded surface plasmon polaritons (SPPs), where the polarization information of light can be reloaded by special SPPs in a controllable way[18–22]. However, most of these devices offer only limited functions in polarization control. To address the ever increasing requirements of information processing, a full polarization generator is one of the desired technologies.

The limitations of polarization control would obviously be overcome with the development of a polarization converter that can convert all polarization states at the same time. However, developing such an all-states polarizer in a single device is quite a challenge. Here, we demonstrate such a plasmonic polarization generator that can generate, in principle, all types of polarizations and route them selectively to the appropriate beams in a controllable way. Due to the interference of the longitudinal field of SPPs, in our design, two orthogonally propagating SPPs are able to provide a collection of all of the near-field polarization states with a regular distribution on a metal surface. These states, therefore, can be individually selected by local scatterers (e.g., nanoholes). Using an appropriate phase modulation, special light beams will be formed with uniform polarization states. Based on this principle, this polarization generator was realized with respect to multiple divided focusing beams. As an impressive manifestation of this polarization generator, eight well-divided focal spots are achieved *simultaneously*, corresponding to eight polarization states (including linear, circular, and elliptical states).

MATERIALS AND METHODS

The polarization reconfiguration process is schematically shown in Figure 1a. Two orthogonal propagating SPPs are launched from a polarized incidence by the L-shaped slit on a metal film with an initial phase lag ($\Delta\varphi_0 = \varphi_x - \varphi_y$) between the x and y directions. Different local phase lags of the two SPPs are reconfigured when they are superposed at different positions of (x, y) as $\Delta\varphi = \Delta\varphi_0 + k_{SPP}(x - y)$. The transverse components of the electric field (E_z) of two orthogonal propagating SPPs, which are both normal to the metal surface, will interfere with each other, resulting in a periodic intensity distribution along the diagonal direction. In contrast, the longitudinal components (the in-plane field, E_x and E_y) are orthogonal to each other and will lead to a series of in-plane polarization states due to the field superposition with respect to different phase lags (see the inset of Figure 1a). Based on this interference of the in-plane fields of SPP waves, all types of the polarization states can be established simultaneously in a plane, which provides a collection of polarizations for further manipulations. By introducing nano-scatterers at the proper locations, a special polarization will be selectively scattered out in a preferred manner. Due to

[1]National Laboratory of Solid State Microstructures, School of Physics, College of Engineering and Applied Sciences, Nanjing University, Nanjing, 210093, China and [2]Collaborative Innovation Center of Advanced Microstructures, Nanjing University, Nanjing 210093, China
Correspondence: T Li, Email: taoli@nju.edu.cn, URL: http://dsl.nju.edu.cn/litao/
Received: 1 January 2015; revised: 27 April 2015; accepted: 6 May 2015; accepted article preview online 12 May 2015

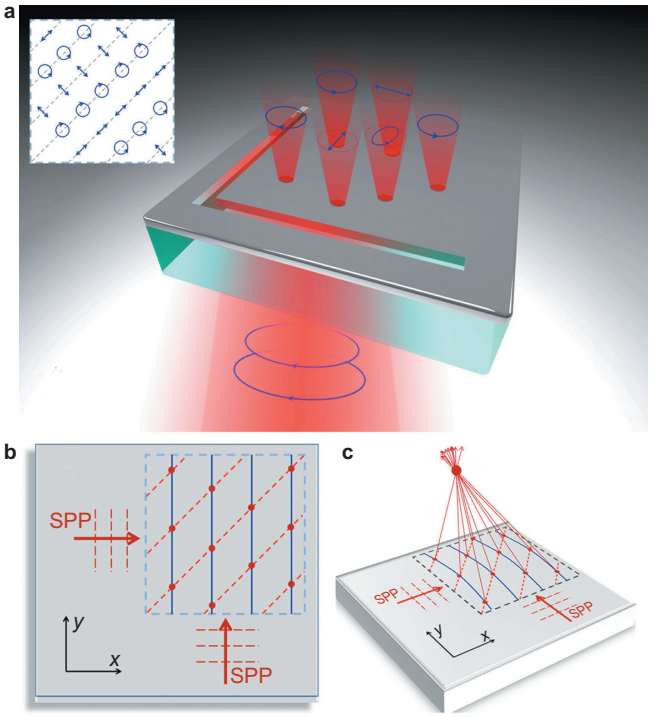


Figure 1 (**a**) Schematic of the polarization reconfiguration process. The inset is the polarization states of the in-plane SPP field distribution with incident RCP light. Design strategy for routing the polarization states to special beams: plane wave scattering (**b**) and focusing beam scattering (**c**).

the nature of dipolar radiation, the amount of scattering from the in-plane components of SPP field (E_x and E_y) is much greater than from the normal one (E_z) to the far-field[23], which ensures the implementation of this polarization router.

To achieve a constructive scattering process to form a desired beam, the phase relation of these scatterers should be carefully designed besides the polarization state, as schematically shown in Figure 1b and 1c. For example, for a SPP propagating in the *x*-direction, the periodic blue straight lines in Figure 1b correspond to a plane-wave scattering, whereas the curved lines in Figure 1c are for a focusing beam. In this article, the focusing beam is designed with the interference principle, that is, all of the scattered lights from the position of the structures (x, y) have the same phase at the focal point of (x_f, y_f, z_f) with respect to SPPs propagating in *x*-direction as

$$k_{SPP}x + k_0 r = c \qquad (1)$$

where k_0 and k_{SPP} are the wavevectors of light in free space and that of SPPs, respectively, $r = \sqrt{(x_f - x)^2 + (y_f - y)^2 + z_f^2}$ and c is a constant. A group of curves with the same phase (or 2π phase lag) will be obtained, as shown in Figure 1c. Returning to the major goal of the polarization generator, the red dashed lines in the diagonal direction represent locations with the same polarization state (same $\Delta\varphi$) and intercept the *y*-axis at values of *y* given by: $\delta = n\lambda_{SPP} + \delta_0$, where n is an integer number, λ_{SPP} is the wavelength of SPP, and δ_0 is the initial intercept which determines a given $\Delta\varphi$. The nano-scatterers are designed to be located at the intersections of the blue curves and red lines, so that they will scatter the local SPP fields out with the same polarization state to form the preferred light beams. These intersections will have the same phase modulation on the other branch of SPP in the *y*-direction because they have the given phase difference $\Delta\varphi$ with the SPP in the *x*-direction, whose contribution is included in the reconfigured polarizations.

Figure 2a displays the optical measurement system used in the experiments. Polarized light from a 633-nm He-Ne laser that is modulated by a polarizer and a quarter-wave plate was focused by an objective lens (4×) and incident normally onto the sample from the backside. The scattered light was analyzed using a polarizer and a quarter-wave plate and then imaged using a CCD camera. Here, we set the fast axis of the incident and analyzing quarter-wave plates as $\pi/4$ with respect to *x*-axis ($\alpha - \beta = -\pi/4$, where α and β are the angles of the fast axis to *x*-axis of the quarter-wave plates in the incident and transmitted sides, respectively). The intensity scattered out from the position (x, y) will be proportional to $\cos^2(\theta_1 - \theta_2 + \Delta\varphi)$, where θ_1 and θ_2 are the angles of axis of the polarizers in the incident and transmitted sides. The detailed determination of the reconfigured polarization state of the scattered beam with respect to the incidence polarization is provided in the Supplementary information.

RESULTS AND DISCUSSION

We first study the case of plane-wave scattering. In this case, the scattered beam has a plane phase front that can be produced from a periodically arranged array of scatterers[24], as illustrated in Figure 1b. The scattered beam satisfies $k_{SPP} - G = k_0 \sin\vartheta$, where $G = 2\pi/a$, a is the period of the scatters in *x*-direction, and ϑ is the diffraction angle of

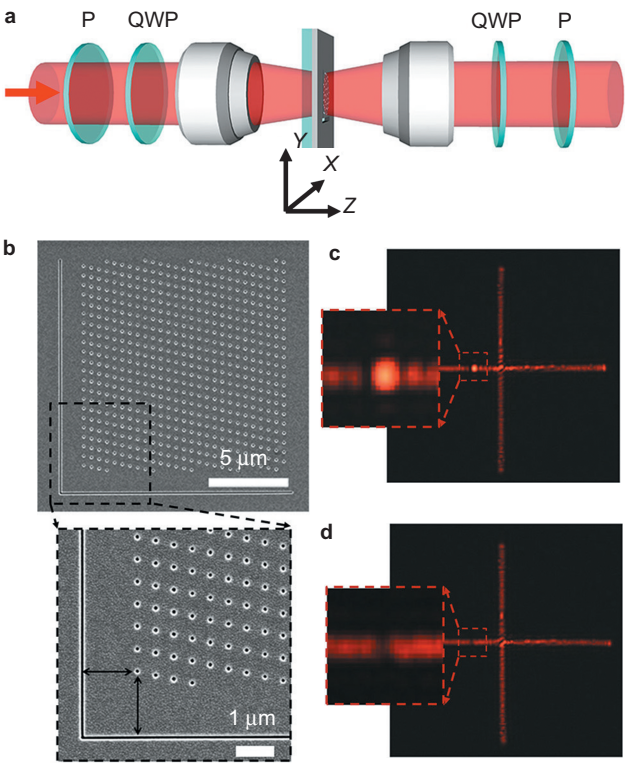


Figure 2 (**a**) Optical setup for the imaging and polarization analyses. (**b**) Scanning electron microscopic (SEM) image of the structure for plane-wave scattering. *a* and *b* are the distances of the first nanohole from the vertical and horizontal slits, respectively. $\delta_0 = b - a = \lambda_{SPP}/2$ is the designed initial intercept to the vertical slit. Images on the Fourier plane with the polarization state selected – LCP (**c**) and unselected – RCP (**d**) with respect to the RCP incident light.

doi:10.1038/lsa.2015.103

the scattered beam. The sample was fabricated using a focused ion beam (FIB, Helios nanolab 600*i*, FEI) instrument on 200-nm thick Ag film, which was sputtered onto a glass substrate. The L-shaped slits used for launching SPPs are 100 nm in width and penetrate through the Ag film. The scatterers within the quadrant area are designed as nanoholes, which were milled with the diameter of 150 nm, depth of 80 nm, and the period of 500 nm in the *x*-direction, as shown in Figure 2b. In fact, a finite area of beam cross section always leads to a Gaussian beam, although it has a plane wave front, so that the scattered light for the plane-wave design corresponds to a Gaussian beam. The scattered light is recorded using a CCD camera in the Fourier plane after the polarization analyzer, where the information of the k-vector beam and its polarization state can be clearly examined. Figure 2c and 2d is the experimental results with respect to a defined nanohole array, with its polarization state being selected and not, respectively. An apparent bright spot is observed, which corresponds to the scattered Gaussian beam in the Fourier plane to be turned on (the upper one) and off (the lower one) (see the zoom-in images in Figure 2c and 2d). As has been interpreted as polarization generator, any polarization state can be generated with respect to the location of the nanohole array on demand by continuously shifting the scatterer array.

In fact, well-routed focusing beams with defined polarization states might be of more practical importance. Our scattering approach does offer a convenient means to achieve the required focusing, as illustrated in Figure 1c. To achieve a symmetric result, one quadrant was extended to four, as shown in Figure 3a. The structures in the left two quadrants (II and III) were designed with the initial intercept of $\delta_0 = \lambda_{SPP}/2$ targeting a focus at the position of (−7.5, 0, 40 μm) on the left side, whereas the right quadrants (I and IV) were designed for the right focus (7.5, 0, 40 μm) with $\delta_0 = 0$. Note that different intercepts correspond to different polarization states in the scattering processes. Therefore, two bright focal spots in the real space were recorded by CCD camera at the focal plane (z = 40 μm) without polarization analysis, as shown in Figure 3b. With polarization analyses, as expected, two orthogonal states are clearly separated (see the spot in Figure 3c for $\delta_0 = \lambda_{SPP}/2$ and the spot in Figure 3d for $\delta_0 = 0$). Note that in the experiments, we used a right-circular polarization (RCP) as the incidence, and its orthogonal state (i.e., left-circular polarization (LCP)) was detected on the left side, with its original RCP was preserved on the right, as shown in Figure 3c and 3d, respectively, according to the different initial intercepts δ_0. The intercept of the hole array indeed determines the generated polarization states for a required diffraction beam, i.e., $\delta_0 = 0$ corresponds to the initial state, $\delta_0 = \lambda_{SPP}/2$ corresponds to the orthogonal one, and $\delta_0 = \lambda_{SPP}/4$ (and $3\lambda_{SPP}/4$) corresponds to the conversion from circular to linear polarizations. Therefore, with the use of a small amount of planar space, any type of polarization state can be achieved, which gives rise to the previously described polarization generator.

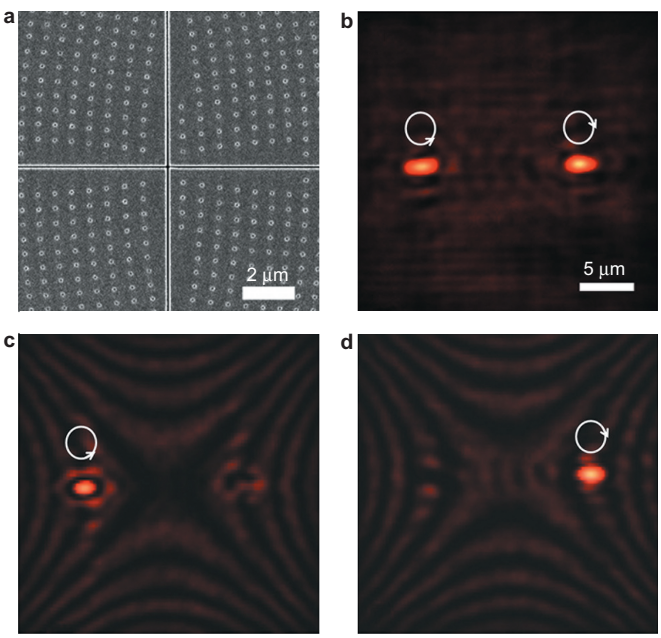


Figure 3 (**a**) SEM image at the center of the nanostructure for the focusing beams. Focus images without polarization analysis (**b**) and analyzed with the polarization states of LCP (**c**) and RCP (**d**).

In fact, a similar concept for the synthesis of light of an arbitrary polarization was demonstrated in a structure composed of a nanoantenna that is connected to dielectric waveguides[25]. The function of this structure, however, is limited to a single output. In our approach, this reconfigurable planar design with a scatterer array had the capability to multiplex, in principle, all types of polarization states in any required beam-forms simultaneously. Here, to manifest this function, we demonstrate an eight-focus polarization generation that is fulfilled by composite nanohole arrays with the spatial multiplexing. The scattered light beams are designed to be focused to the eight vertexes of a right octagon, with respect to the eight different polarization states in the Poincaré sphere. Figure 4a is the SEM image of the sample, showing a composite nano-array. This structure was designed for focusing beams with the focal spots to eight vertices of a right octagon, whose initial intercepts have an equal gap of $\lambda_{SPP}/8$. The various foci are separated into four pairs, with the corresponding structures laid in the four quadrants in sequence. In each quadrant, two sets of nanohole arrays are designed and fabricated according to the two orthogonal polarization states of the light, which have an initial intercept (δ_0) difference of $\lambda_{SPP}/2$ and reveal a mixed feature of superposed hole arrays (see the magnified image in Figure 4a).

The incident polarization is RCP, as is the polarization of the former one (the amplitudes of E_x and E_y are equal), which determines that the designed eight polarization states will be on the great circle of the Poincaré sphere (see Figure 4c). In the measurement, eight foci are clearly recorded in the focal plane (z = 40 μm) with similar intensities without the polarization analyzer, as shown in Figure 4b, where the corresponding designed polarization states are sketched aside. To identify these states, the integrated intensities of the foci with respect to different analyzer conditions (checked by the angles of the polarizer) are plotted in Figure 4d, which shows good agreement with the theoretical predictions of $\cos^2(\theta_1 - \theta_2 + \Delta\varphi)$, where θ_1 is fixed for the RCP incidence and $\Delta\varphi = k_{SPP}\delta_0$ correspond to the eight different states. Here, the focusing results of two typical analyzer conditions are demonstrated as shown in Figure 4e and 4f, corresponding to the dashed lines (u) and (v) in Figure 4d, respectively. The intensities of the foci are clearly distinct, especially those orthogonal pairs (e.g., i and ii in Figure 4e and v and vi in Figure 4f), indicating the realization of the eight polarization states. Therefore, the simultaneous generation of multiple foci with different polarization states on the great circle of the Poincaré sphere is verified. Note that other polarization states on the Poincaré sphere (e.g., on the small circles) also can be achieved by tuning the amplitude ratio of E_x/E_y of incidence, which is also discussed in the Supplementary information.

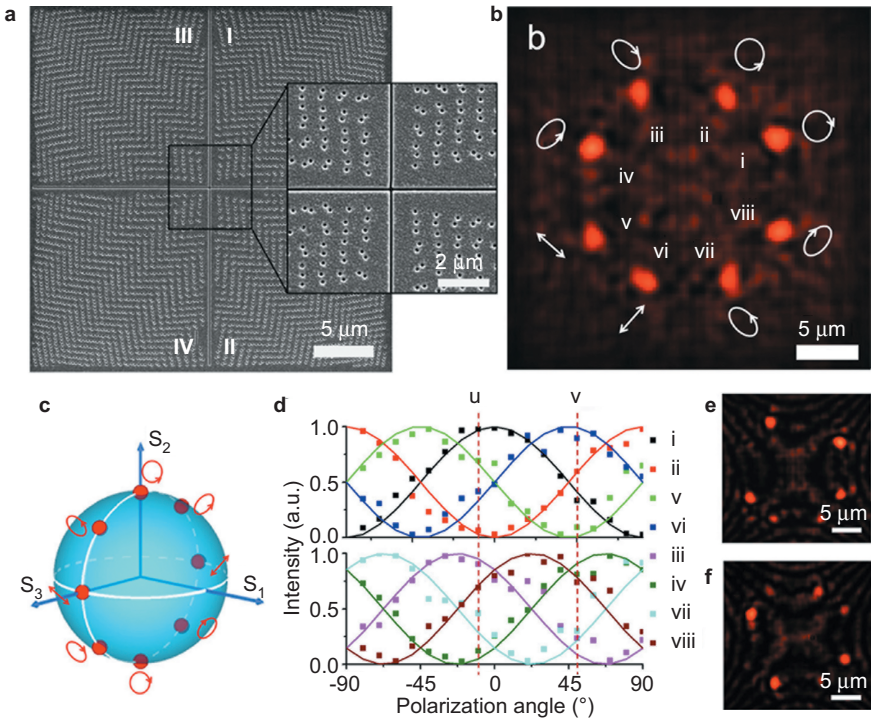


Figure 4 (**a**) SEM image of the polarization generator for the eight-foci process. (**b**) Focus image without polarization analysis. The numerals i to viii represent the eight polarization states of the foci. The corresponding structures for the foci of i and ii, iii and iv, v and vi, vii and viii are laid in the quadrants I, II, III and IV in **a**, respectively. (**c**) The polarization states of the foci on the Poincaré sphere, in which the three Stokes parameters are $S_1 = |E_y|^2 - |E_x|^2, S_2 = 2|E_x||E_y|\mathbf{sin}\delta$, and $S_3 = 2|E_x||E_y|\mathbf{cos}\delta$, which define the entire space of polarization states, and δ is the phase difference between the field components in the *x*- and *y*-axis. (**d**) Symbols for the integrated intensities of the foci at different polarization analysis conditions, and curves for the theoretical prediction. (**e**) and (**f**) Two focus images corresponding to the dashed lines (*u*) and (*v*) in panel (**d**).

Our approach was demonstrated to have the powerful ability to generate multiple routed beams with various polarizations. Compared with the previous techniques for polarization control (polarization rotators, convertor, etc.), our approach does not suffer from the same limitations due to introduction of an intermediate process between the light input and output as the reconfigurable polarization generator, i.e., the orthogonal SPP interference. According to the achieved eight-states-foci, our approach can be adopted in the current multiplexing technique of fiber communications (see the schematic in the Supplementary information). Moreover, this strategy is quite general and adaptable. For example, our approach can be adapted to a unidirectional SPP launching design proposed by Lin *et al.*[20], by which a spatial demultiplexer is added in the polarization generation to provide a complete 2 × 2 polarization division multiplexer (see the Supplementary information). This approach is independent of any resonance, making the entire process relatively low loss and allowing for a further application of the polarization manipulation *via* the resonant design. As a result, our method can provide a new dimension of freedom in manipulating SPPs and light in a manner that can be coexistent with resonance modulation in the metasurface scheme[26,27].

CONCLUSIONS

In summary, we proposed and demonstrated a plasmonic polarization generator that can reconfigure an incident polarization into various polarization states with the desired beam characteristics. The critical process in the plasmonic polarization generator is established by the interference of the orthogonal in-plane fields of two SPPs launched by two crossed slits. Including two orthogonal states, eight polarization states were simultaneously generated and routed to eight foci. Our strategy does not suffer from the limitation of conventional approaches of simplex polarization control, and offers versatile and flexible opportunities to simultaneously tailor the polarization and phase of light. In addition to the revealed polarization generator, this approach is expected to promote the capability of full control of light and even open a new avenue in designing new types of integrated functional photonic devices.

ACKNOWLEDGEMENT

This work was supported by the National Key Projects for Basic Researches of China (No. 2012CB921501) and the National Natural Science Foundation of China (Nos. 11174136, 11322439, 11321063, and 91321312). This work was also supported by the Dengfeng Project B and Outstanding Ph.D. candidate Program A of Nanjing University and the PAPD project of Jiangsu Higher Education Institutions.

1 Koerkamp KK, Enoch S, Segerink F, van Hulst N, Kuipers L. Strong influence of hole shape on extraordinary transmission through periodic arrays of subwavelength holes. *Phys Rev Lett* 2004; **92**: 183901.
2 Gordon R, Brolo A, McKinnon A, Rajora A, Leathem A *et al*. Strong polarization in the optical transmission through elliptical nanohole arrays. *Phys Rev Lett* 2004; **92**: 037401.
3 Yu N, Wang QJ, Pflügl C, Diehl L, Capasso F *et al*. Semiconductor lasers with integrated plasmonic polarizers. *Appl Phys Lett* 2009; **94**: 151101.
4 Ellenbogen T, Seo K, Crozier KB. Chromatic plasmonic polarizers for active visible color filtering and polarimetry. *Nano Lett* 2012; **12**: 1026–1031.
5 Wang L, Li T, Guo R, Xia W, Xu X *et al*. Active display and encoding by integrated plasmonic polarizer on light-emitting-diode. *Sci Rep* 2013; **3**: 2603.

doi:10.1038/lsa.2015.103

6 Zhang J, Zhu S, Zhang H, Chen S, Lo GQ *et al*. An ultracompact surface plasmon polariton-effect-based polarization rotator. *IEEE Photon Technol Lett* 2011; **23**: 1606–1608.
7 Li T, Wang SM, Cao JX, Liu H, Zhu SN. Cavity-involved plasmonic metamaterial for optical polarization conversion. *Appl Phys Lett* 2010; **97**: 261113.
8 Xu J, Li T, Lu FF, Wang SM, Zhu SN. Manipulating optical polarization by stereo plasmonic structure. *Opt Express* 2011; **19**: 748–756.
9 Zhao Y, Alù A. Manipulating light polarization with ultrathin plasmonic metasurfaces. *Phys Rev B* 2011; **84**: 205428.
10 Li T, Liu H, Wang SM, Yin XG, Wang FM *et al*. Manipulating optical rotation in extraordinary transmission by hybrid plasmonic excitations. *Appl Phys Lett* 2008; **93**: 021110.
11 Ginzburg P, Fortuño FJ, Wurtz GA, Dickson W, Murphy A *et al*. Manipulating polarization of light with ultrathin epsilon-near-zero metamaterials. *Opt Express* 2013, **21**: 14907–14917.
12 Afshinmanesh F, White JS, Cai W, Brongersma ML. Measurement of the polarization state of light using an integrated plasmonic polarimeter. *Nanophotonics* 2012, **1**: 125–129.
13 Shitrit N, Bretner I, Gorodetski Y, Kleiner V, Hasman E. Optical spin Hall effects in plasmonic chains. *Nano Lett* 2011; **11**: 2038–2042.
14 Shitrit N, Yulevich I, Maguid E, Ozeri D, Veksler D *et al*. Spin-optical metamaterial route to spin-controlled photonics. *Science* 2013; **340**: 724–726.
15 Yin XB, Ye ZL, Rho J, Wang Y, Zhang X, Photonic spin hall effect at metasurfaces. *Science* 2013; **339**: 1405–1407.
16 Li G, Kang M, Chen M, Zhang S, Pun EY *et al*. Spin-enabled plasmonic metasurfaces for manipulating orbital angular momentum of light. *Nano Lett* 2013; **13**: 4148–4151.
17 O'Connor D, Ginzburg P, Rodríguez-Fortuño FJ, Wurtz GA, Zayats AV. Spin–orbit coupling in surface plasmon scattering by nanostructures. *Nat Commun* 2014; **5**: 5327.
18 Genevet P, Lin J, Kats MA, Capasso F. Holographic detection of the orbital angular momentum of light with plasmonic photodiodes. *Nat Commun* 2012; **3**: 1278.
19 Gorodetski Y, Drezet A, Genet C, Ebbesen TW. Generating far-field orbital angular momenta from near-field optical chirality. *Phys Rev Lett* 2013; **110**: 203906.
20 Lin J, Mueller JB, Wang Q, Yuan G, Antoniou N *et al*. Polarization-controlled tunable directional coupling of surface plasmon polaritons. *Science* 2013; **340**: 331–334.
21 Rodríguez-Fortuño FJ, Marino G, Ginzburg P, O'Connor O, Martínez A *et al*. Near-field interference for the unidirectional excitation of electromagnetic guided modes. *Science* 2013; **340**: 328–330.
22 Miroshnichenko AE, Kivshar YS. Polarization traffic control for surface plasmons. *Science* 2013; **340**: 283–284.
23 Wang J, Zhao C, Zhang J. Does the leakage radiation profile mirror the intensity profile of surface plasmon polaritons? *Opt Lett* 2010; **35**: 1944–1946.
24 Jun YC, Huang KCY, Brongersma ML. Plasmonic beaming and active control over fluorescent emission. *Nat Commun* 2011; **2**: 283.
25 Rodríguez-Fortuño FJ, Puerto D, Griol A, Bellieres L, Martí J *et al*. Universal method for the synthesis of arbitrary polarization states radiated by a nanoantenna. *Laser Photon Rev* 2014; **8**: L27–L31.
26 Yu N, Genevet P, Kats MA, Aieta F, Tetienne JP *et al*. Light propagation with phase discontinuities: generalized laws of reflection and refraction. *Science* 2011; **334**: 333–337.
27 Ni X, Emani NK, Kildishev AV, Boltasseva A, Shalaev VM. Broadband light bending with plasmonic nanoantennas. *Science* 2012; **335**: 427.

This license allows readers to copy, distribute and transmit the Contribution as long as it is attributed back to the author. Readers are permitted to alter, transform or build upon the Contribution as long as the resulting work is then distributed under this or a similar license. Readers are not permitted to use the Contribution for commercial purposes. Please read the full license for further details at - http://creativecommons.org/licenses/by-nc-sa/4.0/

Supplementary information for this article can be found on the *Light: Science & Applications'* website (http://www.nature.com/lsa/).